Bioresource Technology 140 (2013) 199–210

Contents lists available at SciVerse ScienceDirect

Bioresource Technology

journal homepage: www.elsevier.com/locate/biortech

Combustion of peanut and tamarind shells in a conical fluidized-bed combustor: A comparative study

Vladimir I. Kuprianov *, Porametr Arromdee

School of Manufacturing Systems and Mechanical Engineering, Sirindhorn International Institute of Technology, Thammasat University, Pathum Thani 12121, Thailand

HIGHLIGHTS

- Morphology and thermogravimetry of peanut and tamarind shells are investigated.
- Combustion and emission performance of a conical FBC firing these shells is studied.
- Fuel properties and excess air have important effects on the combustor performance.
- High (~99%) combustion efficiency is achievable for firing peanut and tamarind shells.
- Alumina sand can be used to prevent bed agglomeration when burning these biomasses.

ARTICLE INFO

Article history:
Received 10 February 2013
Received in revised form 20 April 2013
Accepted 23 April 2013
Available online 30 April 2013

Keywords:
Peanut/tamarind shells
Fuel morphology and thermogravimetry
Conical fluidized-bed combustor
Alumina bed material
Combustion and emission performance

ABSTRACT

Combustion of peanut and tamarind shells was studied in the conical fluidized-bed combustor using alumina sand as the bed material to prevent bed agglomeration. Morphological, thermogravimetric and kinetic characteristics were investigated to compare thermal and combustion reactivity between the biomass fuels. The thermogravimetric kinetics of the biomasses was fitted using the Coats–Redfern method. Experimental tests on the combustor were performed at 60 and 45 kg/h fuel feed rates, with excess air within 20–80%. Temperature and gas concentrations were measured along radial and axial directions in the reactor and at stack. The axial temperature and gas concentration profiles inside the combustor exhibited sensible effects of fuel properties and operating conditions on combustion and emission performance. High (~99%) combustion efficiency and acceptable levels of CO, C_xH_y, and NO emissions are achievable when firing peanut shells at excess air of about 40%, whereas 60% is more preferable for burning tamarind shells.

© 2013 Elsevier Ltd. All rights reserved.

1. Introduction

Peanuts and tamarind are popular food products in Thailand and other Asian countries. Peanut shells and tamarind shells are major residues from processing peanuts and tamarind fruits collected in these countries on a large scale.

Annually, about 25 million tons of peanuts (or about 70% of the world crop) are produced in Asia, the main suppliers being China and India (USDA, 2013). Taking into account the availability (as about 25 wt.% of total peanut mass) and calorific value (assessed as 16 MJ/kg according to Hanping et al., 2008), the energy potential of peanut shells in Asian countries is estimated to be about 100 PJ per year. Compared to peanuts, the production of tamarind fruits on the Asian continent is much lower, some 400 thousand tons per year, mainly grown in India and Thailand (El-Siddig et al., 2006). Assuming the availability (assessed as 15 wt.% of total fruit mass) and calorific value (about 16 MJ/kg) of tamarind shells, the energy potential of this biomass residue in Asia can be roughly estimated to be 1 PJ per year. As with many other shell-type biomasses exhibiting excellent combustion properties (high reactivity and substantial calorific value), both peanut and tamarind shells can be considered as potential fuels for small-scale heat and power plants (Demirbaş, 2004).

Grate-firing and fluidized-bed combustion systems (combustors and boiler furnaces) are reported to be the main competing options for energy conversion from biomass. Despite some advantages of the grate-firing systems, such as (i) ability of handling high-moisture biomasses with large particles sizes, (ii) load flexibility, (iii) easy maintenance and (iv) low operational costs, the fluidized-bed combustion systems seem to be the most effective option for biomass utilization by offering multiple important benefits, such as wide fuel flexibility, high combustion efficiency and low emissions (Werther et al., 2000; Van Caneghem et al., 2012).

A large number of studies have been devoted to bubbling, vortexing, and circulating fluidized-bed combustion systems for firing

---

* Corresponding author. Tel.: +66 2 986 9009x2208; fax: +66 2 986 9112.
E-mail address: ivlaanov@siit.tu.ac.th (V.I. Kuprianov).

0960-8524/$ - see front matter © 2013 Elsevier Ltd. All rights reserved.
http://dx.doi.org/10.1016/j.biortech.2013.04.086

conventional biomass fuels, such as rice husk, sugar cane bagasse, and woody residues, widely used for heat and power generation (Werther et al., 2000; Permchart and Kouprianov, 2004; Duan et al., 2013; Fang et al., 2004). These studies were mainly focused on combustion and emission performance of the proposed combustion techniques. Some authors pointed out the difficulty in achieving high combustion efficiency when firing high-ash biomass fuels (Permchart and Kouprianov, 2004), while others highlighted the ash-related operational problems, such as bed sintering and agglomeration (leading eventually to system shutdown), generally caused by alkali-based mineral compounds in biomass ash, particularly when using silica sand as the bed material (Lin et al., 2003; Brus et al., 2005; Chirone et al., 2006; Chaivatamaset et al., 2011).

During the past decade, growing attention has been paid to a feasibility of effective utilization of various unconventional biomass fuels, such as nut/fruit shells, olive cake, cotton/palm stalk, and corncobs. Most studies on burning unconventional biomasses have reported high combustion efficiency and acceptable levels of CO, C_xH_y, and NO emissions, basically affected by fuel properties, combustion method and operating conditions (Sun et al., 2008; Han et al., 2008; Chyang et al., 2012). However, due to the specific features of texture, shape, and size of biomass particles, the combustion of some unconventional biomass fuels (e.g., olive cake, apricot and peach stones) is accompanied by high CO and C_xH_y emissions as well as by elevated unburned carbon content in fly ash, which result in deterioration of combustion efficiency (Kaynak et al., 2005; Varol and Atimtay, 2007). When the combustion efficiency of a biomass-fuelled system is below 99%, the emission of highly hazardous polycyclic aromatic hydrocarbons may be recorded at a substantial level, as reported in the study on combustion of coconut shells (Gulyurtlu et al., 2003).

With a typically elevated content of potassium in fuel ash, unconventional biomass fuels are expected to exhibit a high propensity for bed agglomeration. To prevent this undesirable phenomenon, alternative bed materials (e.g., alumina, aluminum-rich materials, dolomite, limestone) can be used to ensure reliable operation of fluidized-bed combustion techniques during the combustion of such biomass fuels (Werther et al., 2000; Sun et al., 2008; Han et al., 2008).

It appears that the combustion and emission performance of a combustion system firing biomass depends on the fuel morphology and chemical structure, basically affecting thermal and combustion reactivity of the biomass. Scanning electron microscopy (SEM) is reported to be an effective technique widely used to investigate the morphology and surface texture of various biomasses via observing the interior of biomass cells and canals as well as their walls. Some studies provided SEM images revealing the microstructure of untreated biomasses and their chemical components, and also morphological changes during biomass pyrolysis and combustion (Gani and Naruse, 2007; Haykiri-Acma et al., 2010; Fernández et al., 2012).

Generally, agricultural residues consist of cellulose, hemicellulose and lignin, and also include some other minor extractives (Demirbaş, 2004). Low volatilization temperatures of these components (190–320 °C for hemicellulose, 280–400 °C for cellulose, and 320–450 °C for lignin) makes agricultural residues to be highly reactive (Fernández et al., 2012). However, some studies revealed an occurrence of lignin decomposition within a substantially wider temperature range (Haykiri-Acma et al., 2010). Volatile matter of biomass is mainly originated from hemicellulose and cellulose, whereas lignin (a complex biopolymer) is a major contributor to formation of fuel char (Haykiri-Acma et al., 2010), the oxidation rate of which is rather low (Fernández et al., 2012).

Much research has been recently addressed the thermogravimetric (TG) and derivative thermogravimetric (DTG) analyses of various biomasses using the TG/DTG technique (Wang et al., 2009; Varol et al., 2010; Yang et al., 2012; Park et al., 2012). With these analyses, the devolatilization behavior and some important combustion characteristics of biomass, such as ignition, peak and burnout temperatures, can be studies and compared between different biomasses. The peak temperature of the DTG curve, corresponding to the highest decomposition rate of biomass, is a measure of fuel reactivity (Varol et al., 2010), whereas the burnout temperature can be used as a key parameter for optimal design of a combustion system.

This comprehensive study was aimed at investigating the combustion of peanut shells (PNS) and tamarind shells (TMS) in a conical fluidized-bed combustor (referred to as ‘conical FBC’) using a relatively small amount of the bed material, which is important when using high-cost alternative bed materials (Kaewklum and Kuprianov, 2008). Alumina sand was employed in this combustor as the bed material in order to prevent bed agglomeration. To facilitate interpretation of empirical findings from the combustion study, morphological, thermogravimetric, and kinetic characteristics of PNS and TMS were investigated prior to combustion tests. Effects of fuel properties and operating conditions on formation and decomposition of major gaseous pollutants (CO, C_xH_y and NO) in different regions of the reactor, as well as on emissions and combustion efficiency of the conical FBC, were compared between the two biomasses.

2. Experimental

2.1. Experimental set up

Fig. 1 shows the schematic diagram of an experimental set up with the conical FBC as well as the design details of the air distributor used in the combustion study. The combustor consisted of a conical module with 40° cone angle and 0.25 m inner diameter at the bottom plane, and five cylindrical modules of 0.5 m height and 0.9 m inner diameter. In each module, the refractory-cement insulation was 50-mm thick lined inside a 4.5-mm-thick metal wall. Gas sampling ports and stationary Chromel–Alumel thermocouples (of type K) were fixed at different levels in the reactor (see Fig. 1a). Using these stationary thermocouples, temperature was monitored along the reactor centerline during start up and combustion tests.

A 25-hp blower supplied air to the combustor through a pipe of 0.1 m inner diameter. A bubble-cap air distributor with thirteen bubble caps (stand pipes) was used to sustain the bed fluidization in the reactor (see Fig. 1b). The bubble caps were arranged in staggered order on the air distributor plate. An individual stand pipe of 32-mm outer diameter had 64 holes (each of 2 mm in diameter) distributed evenly over the pipe outer surface, and also four vertical slots (each of 10 mm × 2 mm sizes) located under the cap with 47 mm diameter. Thus, airflow from each individual stand pipe penetrated into the space between the pipes through the holes and slots in a radial direction, which facilitated a quasi-uniform distribution of total airflow over the plate and prevented occurrence of spouting fluidization regime of the gas–solid bed. Net cross-sectional area of airflow at the distributor exit (calculated as the difference between area of the 250-mm-diameter plate and total area occupied by the caps) was 0.027 m^2.

A screw-type fuel feeder delivered biomass into the conical module at level $Z = 0.6$ m above the air distributor. A three-phase inverter was employed to control the fuel feed rate via varying rotational speed of the feeder.

An ash-collecting cyclone installed downstream from the combustor collected particulates (fly ash) originated from the biomass combustion.

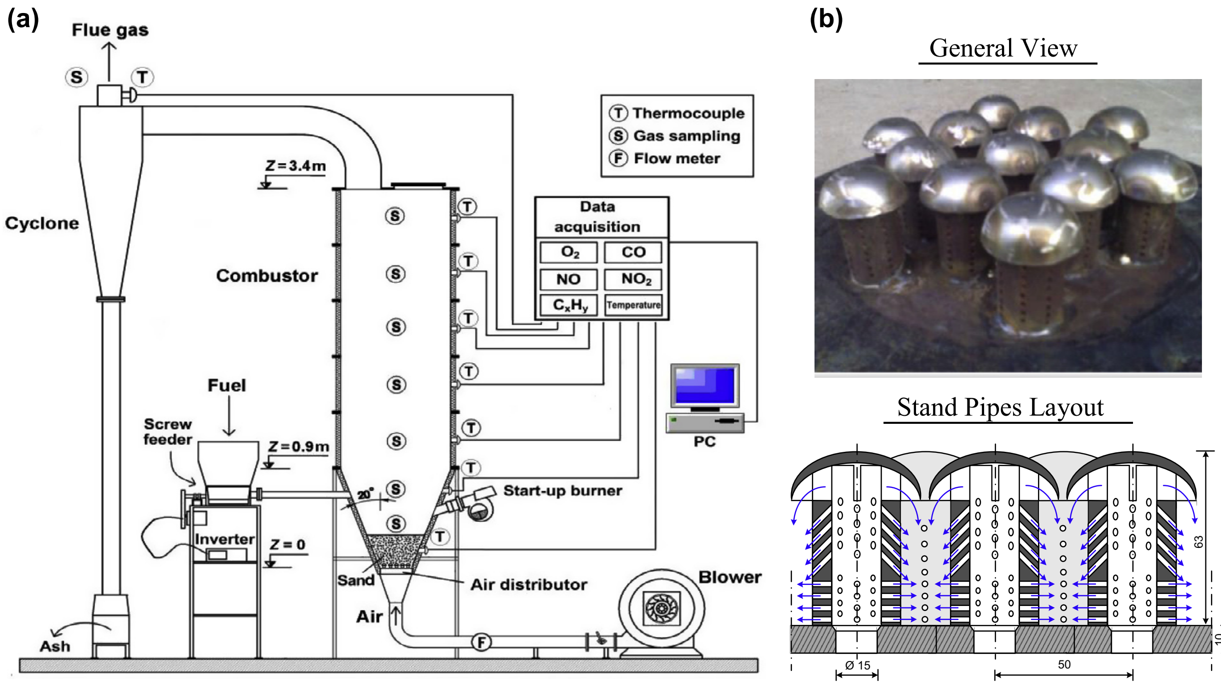

Fig. 1. (a) The experimental set-up with the conical FBC and (b) design details of the bubble-cap air distributor.

2.2. The fuels and the bed material

To achieve higher combustion efficiency and stable fuel feeding, both PNS and TMS were burned as shredded fuels. The shape and size of the shredded biomasses were quite irregular: from dust-like fine particles to flake-shape coarse particles. After shredding, the sieve size of both fuels ranged from 0.1 to 9.5 mm, as found using the ASTM standard method C136-06.

Table 1 summarizes major chemical and physical properties of the biomasses, all being represented by the averages over three repeated analyses/tests. The proximate analysis was performed following ASTM standards D3172–D3175, whereas the ultimate analysis was conducted based on ASTM standards D5373 (for C and H), D3176 (for O), D3177 (for S), and D3179 (for N). It can be seen in Table 1 that both PNS and TMS had a significant content of volatile matter, a moderate proportion of fixed carbon, but rather low contents of fuel moisture and ash. The real (solid) density of each biomass was estimated as the mass-to-volume ratio of a fuel sample. The lower heating value of the fuels was about 16 MJ/kg, as determined following the ASTM standard method D5865. Note that the calorific value of these two unconventional biomass fuels is somewhat higher than that of some viable biomass fuels available in Thailand, such as rice husk and wood sawdust (Permchart and Kouprianov, 2004). From Table 1, PNS contained substantially higher fuel N and had a much greater solid density than TMS. Due to rather low fuel S, SO_2 was not addressed in this study.

Table 1
Properties of biomass fuels used in the combustion studies

Property	Peanut shells	Tamarind shells
Proximate analysis (on as-received basis, wt.%)		
Moisture	9.3	8.6
Volatile matter	65.4	66.8
Fixed carbon	19.6	21.7
Ash	5.7	2.9
Ultimate analysis (on dry and ash-free basis, wt.%)		
C	56.59	53.90
H	6.45	5.92
N	1.53	0.63
O	35.34	39.53
S	0.09	0.02
Structural analysis (on dry and ash-free basis, wt.%)		
Hemi-cellulose	9.7	9.1
Cellulose	46.5	36.9
Lignin	41.3	29.1
Density (kg/m^3)	580	420
Lower heating value (kJ/kg)	16,400	16,300

Table 2 shows the composition of PNS and TMS ashes (as representative oxides, wt.%, averaged over two repeated analyses) determined by X-ray fluorescence (XRF). Along with the compounds in Table 2, the ash analyses included minor/negligible proportions of MnO, SrO, ZrO_2, CuO, BaO, Rb_2O, Na_2O and some other oxides. Silicon, aluminum, potassium and iron were major elements in the PNS ash, whereas calcium and potassium were predominant in the fuel ash of TMS. Elevated (in PNS ash) and significant (in TMS ash) content of K_2O indicated a high tendency to bed agglomeration that would occur during the fluidized-bed combustion of these biomasses if a conventional bed material (silica sand) were used to sustain the bed fludiziation (Werther et al., 2000).

To prevent bed agglomeration, alumina sand with a solid density of about 3400 kg/m^3 and particle sizes of 0.3–0.5 mm was used as the bed material. Table 3 shows the chemical composition of the bed material (as oxides, wt.%, averaged over two repeated analyses) prior to combustion tests. As with the fuel ashes, the X-ray fluorescence (XRF) technique was used to quantify the composition of alumina sand.

2.3. Methods for the morphological, thermogravimetric and kinetic studies

To extend awareness of fuel properties, the morphological, thermogravimetric, and kinetic characteristics of PNS and TMS were investigated prior to combustion tests.

A *JEOL JSM-6400* scanning electron microscope configured with an energy dispersive system (SEM-EDS) was used to examine the internal surface (i.e., surface texture) of biomass particles, likely

Table 2
Composition of fuel ash (wt.%) in peanut and tamarind shells.

Biomass	SiO_2	Al_2O_3	Fe_2O_3	CaO	MgO	SO_3	K_2O	TiO_2	P_2O_5
Peanut shells	39.04	21.92	11.60	6.20	3.26	2.05	11.24	1.60	2.17
Tamarind shells	0.47	1.19	0.25	65.16	5.01	0.85	22.79	0.01	3.45

Table 3
Chemical composition of alumina (wt.%) used as the bed material in the combustor.

SiO_2	Al_2O_3	Fe_2O_3	TiO_2	CaO	MgO	K_2O
3.46	92.42	0.66	2.74	0.72	0.18	0.11

affecting biomass reactivity during the stages of fuel devolatilization and volatile oxidation.

A Mettler-Toledo *TGA/SDTA 851e* thermogravimetric analyzer was employed to obtain the thermogravimetric characteristics (TG and DTG curves). Dry air supplied into the analyzer furnace at a flow rate of 60 ml/min was used as the medium surrounding the biomass sample in the furnace. During the thermogravimetric test with an individual biomass, a 7–10 mg sample was heated from room temperature to 900 °C (or 1173 K). To compare the thermogravimetry of the shells with some reference data, the analyses were performed at a constant heating rate, $\beta = 20$ K/min, and were repeated at least three times for each biomass. Some important combustion characteristics, such as the ignition temperature, the peak temperatures and the burnout temperature (all being used in characterization of fuel reactivity), were obtained from analyses of the TG and DTG curves. Afterwards, the combustion characteristics were averaged over the repeated TGA tests and compared between the two biomass fuels.

The decomposition kinetics of the shells was studied using the Coats–Redfern method successfully approbated by Sun et al. (2010) for determining major kinetic characteristics of biomass decomposition during the thermogravimetric (combustion) tests. Ignoring the process of biomass dewatering, the biomass decomposition rate (α) can be defined as follows:

$$\alpha = \frac{w_0 - w_\tau}{w_0 - w_f} \tag{1}$$

where w_0, w_f, and w_τ are the initial, final and current (at time) weights of the biomass sample.

In general, the kinetic equation can be represented in the form of an "*n*-th" order model describing the biomass decomposition with respect to time as:

$$\frac{d\alpha}{d\tau} = A \exp\left(-\frac{E}{RT}\right)(1-\alpha)^n \tag{2}$$

where *A* is the pre-exponential factor, *E* is the activation energy, *R* is the universal gas constant, and *T* is time-related (current) temperature.

For biomass decomposition at a constant heating rate (β = const), Eq. (2) can be represented as:

$$\frac{d\alpha}{(1-\alpha)^n} = \frac{A}{\beta} \exp\left(-\frac{E}{RT}\right) dT \tag{3}$$

Taking into account the main assumption of the Coats–Redfern method ($2RT/E \ll 1$), and also assuming that the value of *E* is unchanged over a selected temperature range, Eq. (3) after its integration yields:

- for $n = 1$:

$$-\ln\left[-\frac{\ln(1-\alpha)}{T^2}\right] = -\ln\left[\frac{AR}{\beta E}\right] + \frac{E}{RT} \tag{4}$$

- for $n \neq 1$:

$$-\ln\left[\frac{1-(1-\alpha)^{1-n}}{T^2(1-n)}\right] = -\ln\left[\frac{AR}{\beta E}\right] + \frac{E}{RT} \tag{5}$$

The left-hand side of Eq. (4) and Eq. (5) can be designated as *y*. With properly selected *n*, experimental data from a thermogravimetric test can be fitted by a first-order curve:

$$y = a + bx \tag{6}$$

where $x = 1/T$, and *a* designates the first term on the right-hand side of Eq. (4) and Eq. (5).

For variable *x* (or *T*), the curve $y = f(x)$ for the selected *n* can be then plotted on a semi-logarithmic graph with the aim to quantify the kinetic constants in Eq. (2): *E* (by using the fit slope *b*) and *A* (from the expression for *a*).

2.4. Experimental methods for the combustion study

In all combustion experiments, (static) bed height of alumina sand was 30 cm. Prior to tests, alumina bed was pre-heated using a diesel-fired start up burner (Riello Burners Co., Press G24). The burner was fixed at a 0.5 m level above the air distributor and inclined at a −30° angle to the horizontal, as shown in Fig. 1a. When the (alumina) bed temperature reached about 700 °C, the burner diesel pump was turned off. However, during the tests, the burner fan continued to operate (at minimal airflow rate) in order to protect the burner's nozzle head against overheating. Furthermore, a rectangular steel plate with dimensions of 20 cm × 30 cm × 0.5 cm was used for screening the burner from the combustor space, with the aim to avoid impacts of the flame onto the burner and also to exclude penetration of burner air into the reactor during experiments.

The fuel feed rate (FR) and percentage of excess air (EA) were selected as the major operating variables in the combustion study. For each fuel option, combustion tests were performed for two fuel feed rates: 60 kg/h (at rated combustor load) and 45 kg/h (at reduced load). For the rated load, heat input to the combustor was 273 kW_{th} for both biomass fuels, whereas it was 205 kW_{th} during operation at the reduced load.

During the tests with an individual biomass, temperature and concentrations of O_2, CO, C_xH_y (as CH_4), and NO were measured along radial and axial directions in the reactor as well as at the cyclone exit (or at stack) using a "Testo-350XL" gas analyzer (Testo, Germany). At a given point, each parameter was measured at least eleven times to quantify its averaged value over a time interval. The measurement accuracies of temperature and gas concentrations were: ±0.5% for temperature, ±5% for CO within the range of 100–2000 ppm, ±10% for CO higher than 2000 ppm, ±10% for C_xH_y up to 40,000 ppm (when calibrated to CH_4), ±5% for NO, and ±0.2% (vol.%) for O_2.

To minimize the volume of experimental work, the radial and axial profiles of temperature and gas concentrations for each fuel option used in the analysis of formation and decomposition of major gaseous pollutants were compared only between two EA values: 40% and 80%. However, to compare CO, C_xH_y and NO emissions and combustion efficiency of the conical FBC between the biomasses, gas concentrations at the cyclone exit (i.e., at stack) were recorded at both fuel feed rates (60 and 45 kg/h), when ranging EA from 20% to 80% for each combustor load. For the particular test run (operating conditions), the amount of EA was determined according to Basu et al. (2000) using O_2, CO, and C_xH_y (as CH_4) at stack. Unburned carbon content in the fly ash (required for the assessment of associated heat loss) was also obtained for each test run using the ASTM standard method D6316.

2.5. Heat losses and combustion efficiency

In this work, combustion efficiency of the conical FBC was determined using the heat-loss method (Basu et al., 2000). For this combustor with no bottom ash, the heat loss due to unburned carbon, q_{uc} (%), was predicted for each test run using the unburned carbon content in the fly ash (C_{fa}, wt.%), the fuel ash content (A, wt.%), and the fuel lower heating value (LHV, kJ/kg) as:

$$q_{uc} = \frac{32,866}{LHV}\left(\frac{C_{fa}}{100 - C_{fa}}\right)A \qquad (7)$$

The heat loss owing to incomplete combustion, q_{ic} (%), was quantified based on the CO and C_xH_y (as CH_4) emissions from the combustor (in ppm, on a dry gas basis and at 6% O_2) as:

$$q_{ic} = (126.4\,CO + 358.2CH_4)_{@6\%\,O2}10^{-4}V_{dg@6\%\,O2}\frac{(100 - q_{uc})}{LHV} \qquad (8)$$

where $V_{dg@6\%\,O2}$ is the volume of flue gas (on a dry gas basis and at 6% O_2) calculated according to Chakritthakul and Kuprianov (2011) using the ultimate fuel analysis (see Table 1) and the theoretical (stoichiometric) volume of air, the latter being predicted according to Basu et al. (2000).

The combustion efficiency of the fluidized-bed combustors, η_c (%), was then determined using the heat losses estimated by Eqs. (7) and (8) as:

$$\eta_c = 100 - (q_{uc} + q_{ic}) \qquad (9)$$

3. Results and discussion

3.1. Biomass morphology

As revealed by observation of the SEM micrographs, both PNS and TMS biomass samples exhibited a cellular texture of the shells "constructed" from the tightly packed hollow cells of various sizes: from a few microns to about 30 μm. Furthermore, the SEM images of PNS indicated an existence of large-size pores (of up to 200 μm in diameter) in the shell structure and therefore a greater porosity of this biomass compared to TMS.

Like other shell-type biomasses, the cell wall material of PNS and TMS generally consisted of cellulose, hemicellulose, and lignin, as reported in Table 1. Cellulose microfibrils (considered as the structural framework of an individual cell) were embedded in the matrix, generally consisting of hemicellulose and lignin, the latter being the major binding material of the cell wall (Haykiri-Acma et al., 2010). From Table 1, TMS included a substantial amount (about 25%) of extractives, likely represented by some high-molecular biopolymers (e.g., pectins and lipids), which, together with lignin, ensured a hard structure of this biomass compared to the "elastic" particles of PNS.

From the micrographs of the two shells at high (1500×) magnification, a typical cell of each biomass had a very small wall thickness: about 1 μm for PNS and 2–4 μm for TMS. In the meantime, the cell wall of PNS exhibited a large number of small holes (of up to 1 μm in diameter). During volatilization and further oxidation of the wall constituents, these holes may facilitate diffusion (flux) of chemical species in all directions across the shell. Thus, taking into account the highly developed internal surface, high fuel O and also the specifics of a lignocellulosic structure of PNS and TMS (see Table 1), it can be concluded that the thermal and combustion reactivity of the selected biomass fuels is significant. However, thinner cell walls, greater proportion of cellulose in PNS (at nearly the same percentage of hemicellulose in both biomasses) and high structural porosity of PNS point at the potentially higher reactivity of this biomass compared to TMS.

3.2. Thermogravimetric and kinetic analyses of the fuels

Fig. 2 depicts the TG/DTG curves of the selected biomass fuels. It can be seen in Fig. 2 that the TG curves of both PNS and TMS show similar trends, apparently exhibiting four sequent stages (or temperature regions) basically associated with: (1) dewatering of the biomass samples, (2) volatilization of high-reactive chemical components of the shells (cellulose, hemicellulose and partly lignin) accompanied by volatile oxidation, (3) volatilization of the rest lignin and other high-molecular extractives accompanied by oxidation of volatile matter and char, and (4) low-rate oxidation of chars. Some important thermal and combustion characteristics of both fuels, such as the dewatering, ignition, peak and burnout temperatures, were obtained from the TG/DTG analysis as well.

Within the first stage, when temperature gradually increased and attained the dewatering temperature (T_w), fuel moisture was completely vaporized from the biomass sample resulting in dehydration and corresponding weight loss of the sample. From Fig. 2, the dewatering temperature was quite similar for the two biomasses (T_w = 130–140 °C). However, the ignition temperature (T_{ign}) at the point of intersection of two lines related to the TG curve – a horizontal line exhibiting the amount of fuel moisture loss and a tangent line at the maximum rate of the mass loss – was apparently different: T_{ign} = 290 °C for PNS and T_{ign} = 250 °C for TMS.

Within the second and third regions, the DTG curve of each biomass shows two important peaks corresponding to: (1) main peak temperature ($T_{p,1}$) at the highest volatilization rate of biomass

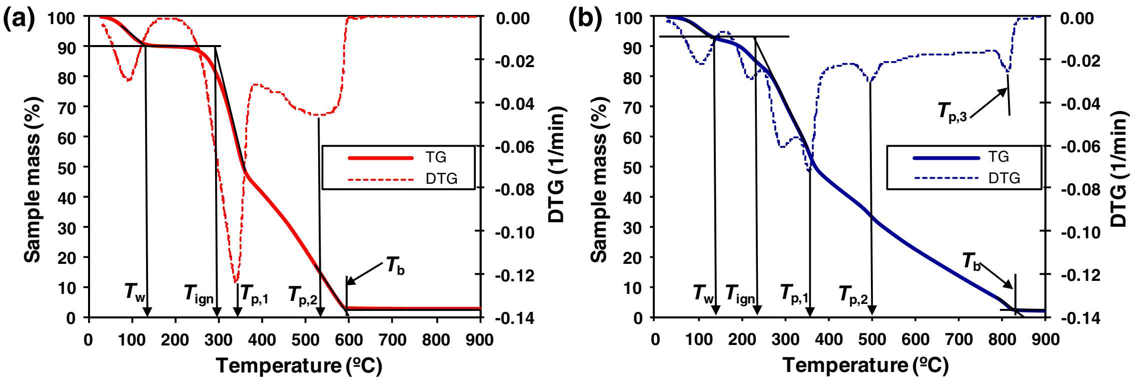

Fig. 2. TG and DTG curves of (a) PNS and (b) TMS samples.

constituents (mainly associated with decomposition of cellulose) and (2) second peak temperature ($T_{p,2}$) basically caused by decomposition of lignin. Two "shoulders" in the DTG curve of TMS within the range between T_{ign} and $T_{p,1}$ indicates the presence in the chemical structure of two highly reactive "light" compounds responsible for the above-mentioned lower value of T_{ign} of TMS compared to PNS. However, the main peak for PNS (335 °C) was apparently lower than that for TMS (350 °C), and this result can be explained by a substantially greater proportion of cellulose in PNS compared to TMS at similar content of hemicellulose in the two biomasses (see Table 1). On the contrary, the second peak temperature of PNS (530 °C) was somewhat higher than that of TMS (500 °C).

In this work, the boundary temperature between the second and third stages was determined as the temperature of complete volatilization of cellulose (T_c), which corresponded to the minimum of the DTG curve located between $T_{p,1}$ and $T_{p,2}$. From Fig. 2, $T_c = 400$ °C for PNS and $T_c = 465$ °C for TMS. As the proportion of lignin in TMS was lower than in PNS, the apparent difference in T_c was likely caused by the presence in TMS of some other (undefined) high-molecular compounds with relatively high volatilization temperature.

Another combustion characteristic, the burnout temperature (T_b) corresponding to the point of intersection of two lines related to the TG curve – a horizontal line indicating the amount of fuel ash (see Table 1) and a tangent line of the TG curve showing the rate of lignin volatilization – was substantially different for the two biomasses: $T_b = 600$ °C for PNS and $T_b = 830$ °C for TMS. It appears that T_b can be treated as the boundary temperature between the third and fourth stages of biomass degradation and oxidation. Note that one more (third) peak temperature was found from TG/DTG analysis of TMS, $T_{p,3} = 820$ °C, likely associated with volatilization of a high-molecular compound, volatilization temperature of which was slightly below T_b.

It can be generally concluded from the thermogravimetric study that with lower $T_{p,1}$ and T_b, PNS can be basically characterized as a biomass of higher thermal and combustion reactivity (in spite of the higher value of T_{ign}) compared to TMS.

Due to air supply into the thermogravimetric system, all volatiles released during the second and third stages were oxidized and continuously removed from the system. The biomass char was also oxidized at a noticeable rate during the third stage, as the residual matter from the TG tests was fuel ash. However, within the last (fourth) stage, i.e., at temperatures greater T_b, the char was likely oxidized without flame and therefore exhibited a very low decomposition rate.

The specific temperatures of PNS and TMS are summarized in Table 4 and compared with reference data for some selected agricultural and wood residues.

Table 5 shows the kinetic characteristics (E, A, and n) of PNS and TMS, which can be used for modeling the time-domain decomposition of the two biomasses by Eq. (2). For more accurate fitting of the experimental data, the kinetic characteristics were determined for distinct temperature regions, with corresponding peaks and "shoulders" in the DTG curve of each biomass (see Fig. 2).

At relatively low temperatures (up to 330 °C), the value of E for TMS (71–84 kJ/mol) was substantially lower than that for PNS (140 kJ/mol), so TMS can be ignited much easily than PNS. This result explains the above-mentioned difference in T_{ign} between the two biomasses. However, at temperatures over 400 °C, PNS was characterized by the lower values of E, which compared to TMS resulted in a faster decomposition rate of biomass lignin and eventually shorter overall time of PNS degradation.

At temperatures below 440 °C, the reaction order n of the two biomasses exhibited rather high values (5–7), however comparable with those (5.0–5.3) of oil palm residues (Khan et al., 2011). At higher temperatures (mainly associated with biomass lignin decomposition and char oxidation), the reaction order of the two biomasses was characterized by conventional values.

3.3. Radial distribution of temperature and gas concentrations in the conical FBC

Fig. 3 shows the radial profiles of temperature and gas concentrations (O_2, CO, C_xH_y and NO) at two different levels (Z) above the air distributor in the conical FBC fired with PNS or TMS at similar operating conditions (60 kg/h fuel feed rate and 40% excess air). It can be seen in Fig. 3 that the radial temperature profiles of the two fuels were quite uniform at both levels, thus pointing at a high rate of heat-and-mass transfer in the radial direction, whereas the gas concentration profiles exhibited rather good uniformity, indicating high intensive gas–solid and gas–gas mixing across the reactor. Such an appearance of the radial profiles allowed using the axial profiles of temperature and gas concentrations for the analysis of combustion and emission performance of the conical FBC.

3.4. Axial temperature and O_2 concentration profiles

Fig. 4 compares the axial temperature and O_2 concentration profiles in the conical FBC between the biomass fuels and operating conditions. In all the trials, the axial temperature profiles were found to be quasi-uniform, exhibiting however (i) a slight positive axial gradient in the reactor conical section ($Z < 0.9$ m), likely caused by endothermic devolatilization of fuel in this region as well as by carryover of fine chars into the freeboard (to be addressed below), and (ii) an insignificant negative gradient in the combustor freeboard, basically due the heat loss across combustor walls. In all the test runs, O_2 diminished gradually along the reactor height; however, a predominant proportion of O_2 was consumed in the conical module during the combustion of each biomass, thus pointing at significant fuel burnout in this region.

Table 4
Comparison of thermogravimetric characteristics of some agricultural and wood residues.

Fuel	Heating rate (°C/min)	Temperature (°C)						References
		Dewatering	Ignition	Peak 1	Peak 2	Others peaks	Burnout	
Cotton stalk	20	105	220	260	360	–	505	Sun et al. (2010)
Wood chips	20	–	180	310	360	–	730	Varol et al. (2010)
Olive cake	20	–	190	330	440	770	880	Varol et al. (2010)
Hazelnut shells	20	–	185	330	370	440,760	860	Varol et al. (2010)
Tobacco stem	20	–	250	300	380	520	600	Yang et al. (2012)
Straw dust	15	130	280	350	430	–	–	Wang et al. (2009)
Wheat straw	15	120	280	320	–	–	–	Wang et al. (2009)
Peanut shells	20	130	290	335	530	–	600	Current study
Tamarind shells	20	140	250	350	500	820	830	Current study

Table 5
Fitting equation and kinetic parameters of peanut/tamarind shells for different temperature ranges.

Sample	Temperature range (°C)	Fitting equation	Correlation coefficient (r)	Activation energy (E (kJ/mol))	Pre-exponential factor (A (1/min))	Reaction order (n)
Peanut shells	200–390	$y = -15.40 + 16.85x$	0.9972	140	1.64×10^{12}	7
	390–440	$y = -0.5433 + 7.877x$	0.9971	65.5	2.71×10^{5}	5
	440–600	$y = 8.913 + 3.245x$	0.9769	27.8	8.74	0.7
Tamarind shells	160–250	$y = -5.483 + 10.16x$	0.9926	84.4	4.89×10^{7}	6.5
	250–330	$y = -1.759 + 8.545x$	0.9944	71.1	9.92×10^{5}	7
	330–440	$y = -2.968 + 9.081x$	0.9832	75.5	3.53×10^{6}	7
	440–830	$y = 8.345 + 3.353x$	0.9556	32.9	15.9	2

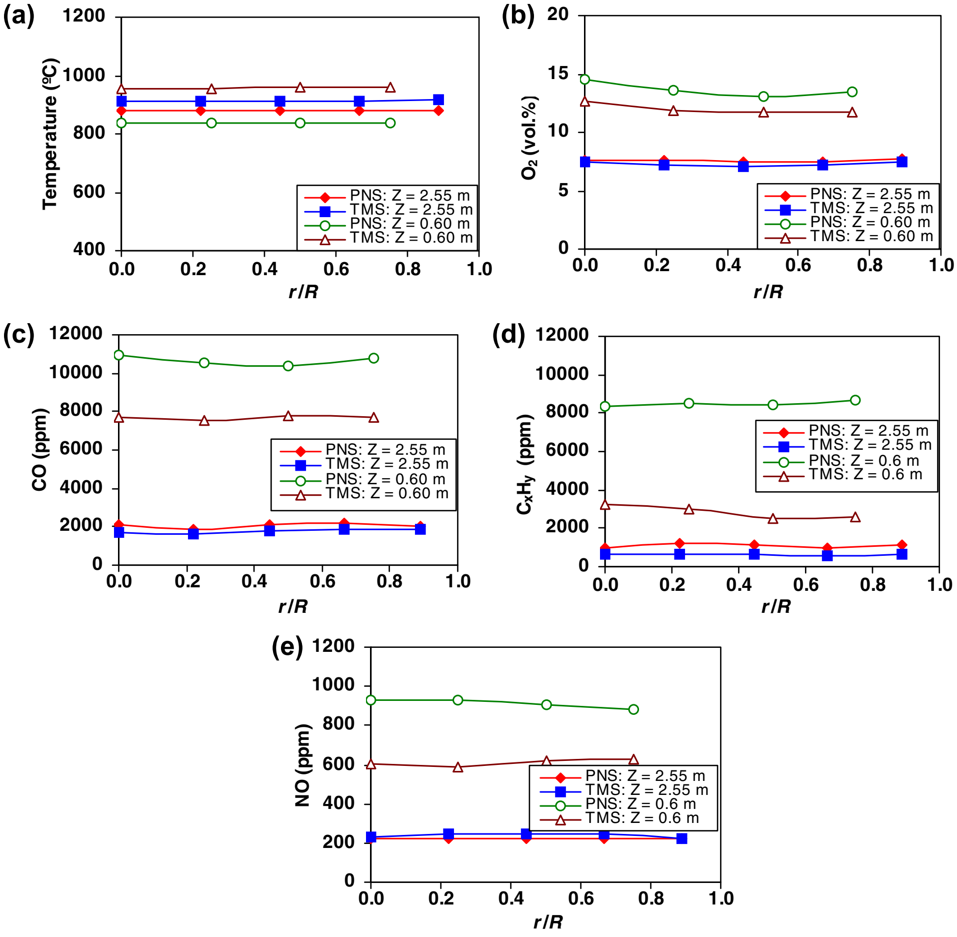

Fig. 3. Radial (a) temperature and (b) O_2, (c) CO, (d) C_xH_y, and (e) NO concentration profiles at different levels above the air distributor in the conical FBC when firing 60 kg/h peanut/tamarind shells at excess air of 40%.

3.4.1. Effects of fuel type and properties

Despite higher thermal and combustion reactivity of PNS revealed by the morphological and thermogravimetric studies, temperature at any point in the bottom region of the combustor fired with this biomass turned out to be noticeably lower compared to burning of TMS at similar operating conditions. This result was likely caused by an elevated carryover of PNS chars from this region. When entering the combustor at $Z = 0.6$ m, particles of this biomass with thinner cell walls and greater porosity (revealed by the morphological study) were devolatilized and destructed almost instantaneously forming fine chars, a certain proportion of those was carried out into the freeboard contributing to higher heat release in the cylindrical part of the combustor. On the contrary, due to lower thermal reactivity of TMS (as found in the TG/DTG analysis), the particles of this biomass with greater thickness of cell walls can form chars with greater particle sizes, which, compared to PNS, led to their deeper penetration into the fluidized bed and therefore greater contribution to heat release in the reactor bottom. However, higher fuel moisture and lower proportion of volatile matter in PNS were only minor factors for the temperature difference between the biomasses.

At first glance, an influence of the fuel type on the axial O_2 concentration profiles was rather weak. However, during the combustion of TMS, the consumption of O_2 at the reactor bottom was noticeably greater than that when burning PNS at similar operating conditions, whereas PNS exhibited a higher rate of O_2 consumption

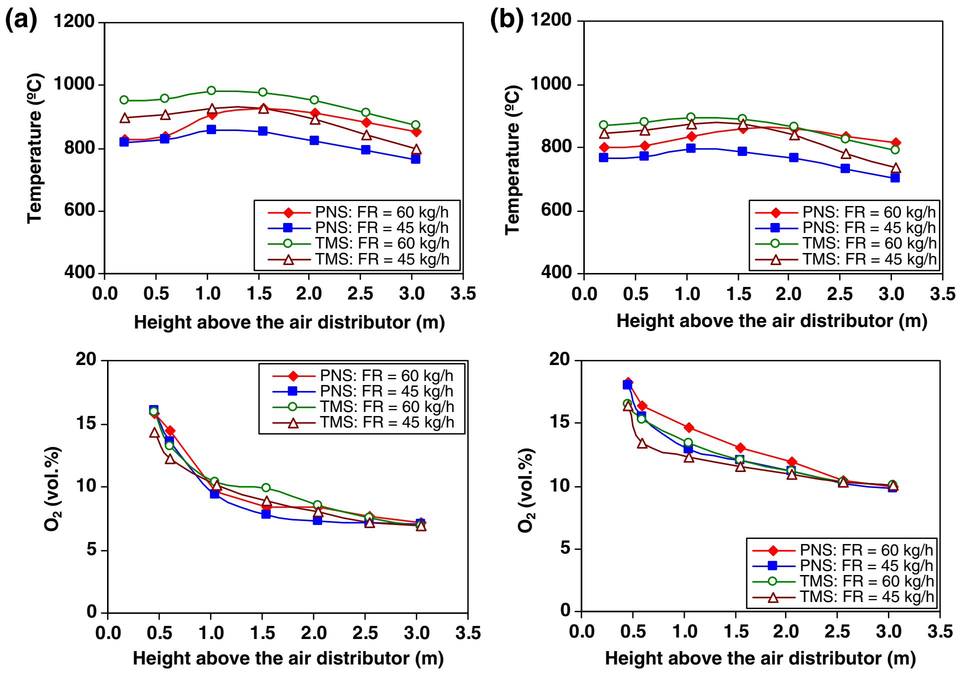

Fig. 4. Effects of the fuel feed rate on the axial temperature and O_2 concentration profiles in the conical FBC when firing peanut/tamarind shells at excess air of (a) 40% and (b) 80%.

in the freeboard. Such behavior of O_2 was in agreement with the previously discussed temperature profiles.

3.4.2. Effects of operating conditions

Experimental results in Fig. 4 revealed that with reducing the combustor load, temperature at the reactor bottom was somewhat lowered at all locations, as the heat release due to the combustion diminished more rapidly than the heat transfer (or heat loss) across the reactor walls (Basu et al., 2000). In the meantime, a load reduction (at fixed EA) led to a greater rate of O_2 consumption and consequently greater fuel burnout in this region (despite the reduction in bed temperature), mainly due to the increase in residence time of the reactants.

An increase in excess air (at fixed combustor load) resulted in some reduction of temperature at all locations inside the rector, mainly due to the dilution effect of excessive air. Despite some differences in the rate of O_2 consumption in the combustor bottom during the combustion of PNS and TMS, O_2 diminished in the freeboard to a single value at the combustor top, which was almost independent of the fuel type and combustor load but solely affected by a specified amount of excess air, as can be compared in Fig. 4a and b.

3.5. Formation and decomposition of major gaseous pollutants along the axial direction

Fig. 5 shows the axial CO, C_xH_y and NO concentration profiles for the same fuel options and operating conditions, as in Fig. 4. In all the test runs, these profiles exhibited two specific regions inside the reactor with different net results of pollutants formation/decomposition.

In the first region, below the level of fuel injection ($0 < Z < 0.6$ m), both CO and C_xH_y showed a significant increase along the axial direction, mainly due to rapid devolatilization of fuel particles, accompanied however by oxidation of volatile CO and C_xH_y as well as of chars (Turns, 2006). Basically, oxidation of CO to CO_2 occurred through a sequence of chain reactions involving O_2 and water vapor (OH radicals), whereas decomposition of C_xH_y proceeded mainly via two groups of intermediate reactions: (i) oxidation of C_xH_y to CO, and afterward (ii) oxidation of CO to CO_2. Char carbon was likely oxidized via four major routes (involving O_2, CO_2 and OH) resulting in formation of CO followed by its conversion to CO_2. In the second region ($Z > 0.6$ m), where the decomposition reactions were predominant, both CO and C_xH_y showed a diminishing trend along the combustor height, and eventually quite low values at the combustor top.

Like CO and C_xH_y, the axial NO concentration profiles exhibited two specific regions. In the first region ($0 < Z < 0.6$ m), the rate of NO formation from nitrogenous volatile species (mainly, NH_3) was higher than rate of NO decomposition occurred basically via catalytic reaction of NO with CO on a surface of fuel chars (Werther et al., 2000) and also through homogeneous reactions of NO with NH_3 and light hydrocarbon radicals (Winter et al., 1999; Turns, 2006). In the second region ($Z > 0.6$ m), the rate of chemical reactions responsible for NO decomposition (such as catalytic reduction of NO by CO on the surface of char/ash particles as well as homogeneous reactions of NO with C_xH_y remaining in the flue gas) was likely higher than formation rate of NO, and this resulted in the substantial diminishing of NO along the combustor height. The experimental results in Fig. 5 revealed that the rate of NO decomposition at $0.6\text{ m} < Z < 2$ m was substantial, mainly due to elevated CO and C_xH_y in this region, whereas at $Z > 2$ m, NO exhibited a low-rate decline, since CO and C_xH_y in this region were rather low.

3.5.1. Effects of fuel type and properties

The most important effects of fuel type and properties on the behavior of CO and C_xH_y in the reactor were observed at the rated combustor load and lower level of excess air. It can be seen in Fig. 5a that when firing PNS at FR = 60 kg/h and EA = 40%, the axial gradient of CO and C_xH_y within the first region ($0 < Z < 0.6$ m) was substantially greater than that for burning TMS at similar operating conditions, which resulted in higher peaks of these pollutants in the vicinity of fuel injection. Such a result can be explained by a higher degradation (devolatilization) rate of PNS (revealed by the TG/DTG analysis) and lower rates of the above-mentioned sec-

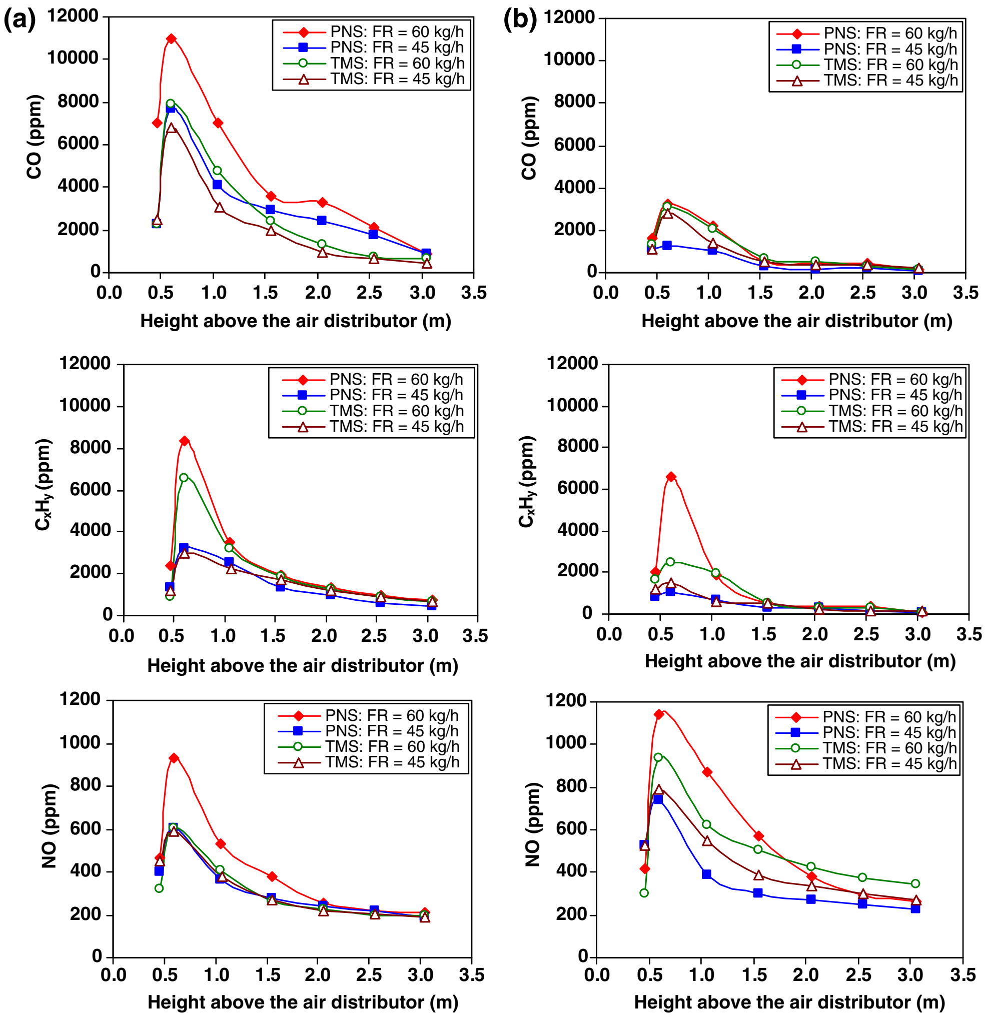

Fig. 5. Effects of the fuel feed rate on the axial CO, C_xH_y (as CH_4) and NO concentration profiles in the conical FBC when firing peanut/tamarind shells at excess air of (a) 40% and (b) 80%.

ondary (oxidation) reactions caused by lower temperatures in this region when burning this biomass. However, at all locations in the second region ($Z > 0.6$ m), a substantially higher level of CO for firing PNS was mainly caused by the (above-addressed) elevated carryover of char particles into the reactor freeboard where char-C was oxidized to CO. Higher fuel moisture and hydrogen in PNS (see Table 1) led to a greater yield of OH radicals during the combustion of PNS and consequently higher rates of CO and C_xH_y oxidation in this region, compared to burning TMS.

When firing PNS, due to elevated fuel N in PNS (see Table 1), causing a greater yield of nitrogenous volatiles, the NO axial gradient in the first region and consequently the peak of NO (at Z 0.6 m), were substantially higher than those for burning TMS at similar operating conditions, despite the higher levels of CO and C_xH_y responsible for the NO reduction. However, during the combustion of PNS, a decreased rate of NO in the upper region was substantially higher than that for TMS (particularly, at the rated combustor load). This was mainly due to the greater fuel ash in PNS (ensuring higher concentration of the catalysts – chars and ash particles – in flue gas) as well as higher CO and C_xH_y at different points in this region.

3.5.2. Effects of operating conditions

At the reduced combustor load, despite the reduction in bed temperature (see Fig. 4), CO and C_xH_y at different locations inside the reactor were lowered for both biomasses, mainly due to the increased residence time. Switching the combustor to firing both fuels at a higher amount of excess air led to a substantial decrease of the CO and C_xH_y peaks (or diminishing of axial CO and C_xH_y gradients within the first region) at both combustor loads (see Fig. 5b), basically due to the enhanced oxidation rate of CO and C_xH_y. However, when firing PNS at the reduced combustor load and higher excess air (EA = 80%), the peaks of CO and C_xH_y were lower than those for TMS (both accounting for about 1000 ppm), which can be explained by the increased effects of higher thermal reactivity of PNS caused due to decreased carryover of PNS chars from the first region into the freeboard.

During the combustion of PNS/TMS, NO at any point in the first region was found to be increased (resulting in the higher peak of NO for each biomass) as the fuel feed rate and/or excess air increased. These effects of operating variables together with the above-mentioned influence of fuel N on the behavior of NO in the combustor bottom confirmed the occurrence of the fuel-NO formation mechanism in this conical FBC (Winter et al., 1999; Turns, 2006; Qian et al., 2011), revealing the proportional correlations of NO with excess air, fuel N, and fuel feed rate (via bed temperature). In the upper region, the diminishing gradient of NO was proportional with the NO peak (affected by processes in the combustor bottom) and was also affected by the fuel type and properties. When burning PNS and TMS at EA = 40% (see Fig. 5a), NO at the combustor top ($Z = 3.1$ m) was weakly dependent on the fuel type and feed rate. However, when switching the combustor to burning these shells at EA = 80%, NO at this location was apparently higher (despite the air dilution effects), thus exhibiting a substantial influence of excess air, but rather weak effects of the fuel type and combustor load on the net NO formation/decomposition in this combustor.

3.6. Emissions and combustion efficiency of the conical FBC

Fig. 6 shows the CO, C_xH_y and NO emissions (all on a dry gas basis and at O_2 = 6%) from the conical FBC when firing the shells at different fuel feed rates for the specified range of excess air. These emission characteristics exhibit, in effect, a net result of pollutant formation and decomposition in distinct regions inside the combustor, where these processes were affected by the fuel properties and operating conditions.

At similar operating conditions, the CO and C_xH_y emissions from burning PNS were noticeably lower than those for firing TMS. Such a result can be explained by the (previously addressed) higher rates of CO and C_xH_y oxidation in the upper part of the combustor when firing PNS (see Fig. 5). Despite that the fuel N in PNS was significantly greater than in TMS, the NO emissions of the two biomasses showed an insignificant difference, mainly due to the above-mentioned higher rate of NO decomposition in the reactor freeboard during the combustion of peanut shells.

It can be seen in Fig. 6 that the CO, C_xH_y and NO emissions of each biomass fuel exhibited substantial effects of excess air, whereas the combustor load had minor effects on the emission characteristics, particularly when firing TMS. The CO and C_xH_y emissions can be reduced via increasing EA, while the NO emission control requires minimizing the amount of excess air. With reducing combustor load (at fixed EA), the gaseous emissions were somewhat lowered, basically due to the increased residence time.

Table 6 shows the predicted heat losses and combustion efficiency of the conical FBC fired with peanut/tamarind shells at actual operating conditions. Parameters required for estimating the amount of excess air and predicting the heat losses for each test run, such as unburned carbon content in the fly ash and concentrations of O_2, CO and C_xH_y (as CH_4) at stack, are provided in Table 6 as well.

Because of the relatively small amounts of fuel ash and unburned carbon content in the fly ash, the heat loss due to unburned carbon of the two biomasses was quite low and had therefore minor effects on the heat balance of the conical FBC. Despite the decrease in combustion temperature and residence time of chars, this heat loss showed the trend to decrease with increasing excess air, likely due to the increased oxidation rate of char-C. However, at fixed excess air, this index was greater for the reduced load, and this was generally caused by the decreased combustion temperature.

From Table 6, the combustion efficiency was mainly influenced by the heat loss due to incomplete combustion. According to Eq. (8), this heat loss was in a proportional correlation with the CO and C_xH_y emissions, and was therefore strongly affected by excess air at fixed combustor load (see Fig. 6). Note that this combustor characteristic was weakly dependent on the fuel type and combustor load, especially at elevated values of EA (60–80%) when the CO and C_xH_y emissions of the fuels were reduced to rather low levels, leading to high combustion efficiency: 99.7–99.8% for firing PNS, and 99.3–99.7% for firing TMS.

Following the behavior of the heat losses, the combustion efficiency showed a trend to increase with increasing excess air within the specified range, whereas the combustion efficiency was almost independent of the fuel feed rate (due to the opposite response of the two heat losses to load variation). It can be consequently concluded that compared to burning TMS, the higher thermal and combustion reactivity of PNS (revealed by the morphological and thermogravimetric studies) resulted in an insignificant improvement of the combustion efficiency of this conical FBC, particularly when operated at elevated excess air.

The national emission limits of 740 ppm for CO and 205 ppm for NO (on a dry gas basis and at 6% O_2) recommended for industrial biomass-fuelled applications by the Pollution Control Department of Thailand (PCD, 2013) were taken into account to quantify an "optimal" (or "compromise") value of excess air for firing PNS

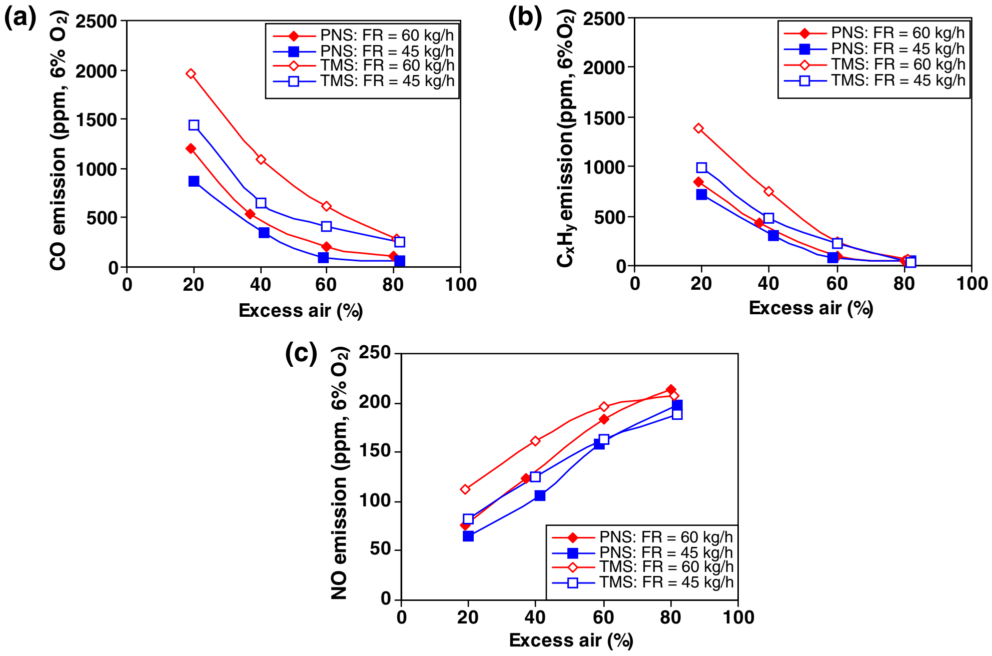

Fig. 6. Comparison of the (a) CO, (b) C_xH_y (as CH_4), and (c) NO emissions of the conical FBC between peanut and tamarind shells fired at the fuel feed rates of 60 and 45 kg/h for similar ranges of excess air.

Table 6
Unburned carbon in the fly ash, concentrations of O_2, CO and C_xH_y (as CH_4) at stack, and predicted heat losses and combustion efficiency of the conical FBC when firing the shells at variable operating conditions.

Excess air (%)	Airflow rate[a] (Nm^3/s)	Carbon in fly ash (wt.%)	O_2 (vol.%)	CO[b] (ppm)	C_xH_y[b] (ppm)	Heat loss (%) due to:		Combustion efficiency (%)
						Unburned carbon	Incomplete combustion	
Firing 60 kg/h peanut shells								
19	0.094	1.98	3.5	1200	840	0.23	1.80	98.0
37	0.108	1.89	5.8	537	434	0.22	0.89	98.9
60	0.126	0.91	7.9	200	92	0.10	0.23	99.7
80	0.142	0.86	9.3	109	54	0.10	0.13	99.8
Firing 45 kg/h peanut shells								
20	0.071	2.94	3.7	874	720	0.35	1.46	98.2
41	0.083	1.12	6.2	352	305	0.13	0.61	99.3
59	0.094	1.12	7.8	100	80	0.13	0.16	99.7
82	0.108	1.01	9.5	59	44	0.12	0.09	99.8
Firing 60 kg/h tamarind shells								
19	0.089	0.96	3.8	1962	1380	0.06	2.82	97.1
40	0.104	0.89	6.2	1091	750	0.05	1.55	98.4
60	0.119	0.98	7.9	610	240	0.06	0.62	99.3
81	0.135	0.97	9.5	291	60	0.06	0.22	99.7
Firing 45 kg/h tamarind shells								
20	0.067	3.89	3.8	1439	993	0.24	2.04	97.7
40	0.078	2.90	6.2	650	470	0.18	0.95	98.9
60	0.089	2.04	7.9	410	217	0.12	0.49	99.4
82	0.102	2.03	9.5	260	26	0.12	0.16	99.7

[a] Under standard conditions: at 1 atm and 0 °C.
[b] On a dry gas basis and at 6% O_2.

and TMS. To reduce environmental impacts of NO_x (a more harmful pollutant than CO) as well as the potential heat loss with waste gas of a boiler that could be integrated with the proposed combustor, it is suggested to select excess air at a minimum possible level, meeting however the above-mentioned emission standard for CO. Following this approach, EA = 40% seems to be the best option for firing PNS, whereas EA = 60% is more appropriate for burning TMS. Under these operating conditions, high (about 99%) combustion efficiency can be achieved, while controlling major (CO and NO) emissions at values below the national emission limits and maintaining simultaneously C_xH_y at a reasonable level (substantially below CO).

Note that during these (~60 h) experimental tests for firing PNS and TMS, no evidence of bed agglomeration was found in the conical FBC using alumina as the bed material. As revealed by visual inspections, the bed material exhibited normal appearance (grains) and ability to fluidize for the entire time period of the combustion experiments.

4. Conclusion

The conical fluidized-bed combustor can be used for effective burning peanut/tamarind shells for wide ranges of fuel feed and excess air. Fuel properties and operating conditions have important effects on formation/decomposition of major gaseous pollutants, combustion efficiency, and emissions of the combustor. Excess air of 40% is the best option for firing peanut shells, whereas 60% is more appropriate for tamarind shells. High (~99%) combustion efficiency can be achieved, while controlling the emissions at acceptable/reasonable levels. By using alumina as the bed material, bed agglomeration can be prevented when burning the shells in this combustor.

Acknowledgements

The authors would like to acknowledge the financial support from Thammasat University (Thailand) as well as from the Thailand Research Fund. The authors are also thankful to the Department of Animal Science, Kasetsart University (Thailand) for the structural analysis of the biomasses used in this study.

References

Basu, P., Cen, K.F., Jestin, L., 2000. Boilers and Burners. Springer, New York.

Brus, E., Öhman, M., Nordin, A., 2005. Mechanisms of bed agglomeration during fluidized-bed combustion of biomass fuels. Energy & Fuels 19, 825–832.

Chaivatamaset, P., Sricharoon, P., Tia, S., 2011. Bed agglomeration characteristics of palm shell and corncob combustion in fluidized bed. Applied Thermal Engineering 31, 2916–2927.

Chakritthakul, S., Kuprianov, V.I., 2011. Co-firing of eucalyptus bark and rubberwood sawdust in a swirling fluidized-bed combustor using an axial flow swirler. Bioresource Technology 102, 8268–8278.

Chirone, R., Miccio, F., Scala, F., 2006. Mechanism and prediction of bed agglomeration during fluidized bed combustion of a biomass fuel: effect of the reactor scale. Chemical Engineering Journal 123, 71–80.

Chyang, C.S., Duan, F., Lin, S.M., Tso, J., 2012. A study on fluidized bed combustion characteristics of corncob in three different combustion modes. Bioresource Technology 116, 184–189.

Demirbaş, A., 2004. Combustion characteristics of different biomass fuels. Progress in Energy and Combustion Science 30, 219–230.

Duan, F., Chyang, C.S., Lin, C.W., Tso, J., 2013. Experimental study on rice husk combustion in a vortexing fluidized-bed with flue gas recirculation (FGR). Bioresource Technology 134, 204–211.

El-Siddig, K., Gunasena, H.P.M., Prasad, B.A., Pushpakumara, D.K.N.G., Ramana, K.V.R., Vijayanand, P., Williams, J.T., 2006. Tamarind, *Tamarindus Indica*. Southampton Centre for Underutilised Crops, Southampton, UK.

Fang, M., Yang, L., Chen, G., Shi, Z., Luo, Z., Cen, K., 2004. Experimental study on rice husk combustion in a circulating fluidized bed. Fuel Processing Technology 85, 1273–1282.

Fernández, R.G., García, C.P., Lavín, A.G., Bueno de las Heras, J.L., 2012. Study of main combustion characteristics for biomass fuels used in boilers. Fuel Processing Technology 103, 16–26.

Gani, A., Naruse, I., 2007. Effect of cellulose and lignin content on pyrolysis and combustion characteristics for several types of biomass. Renewable Energy 32, 649–661.

Gulyurtlu, I., Karunaratne, D.G.G.P., Cabrita, I., 2003. The study of the effect of operating parameters on the PAH formation during the combustion of coconut shell in a fluidised bed. Fuel 82, 215–223.

Han, J., Kim, H., Minami, W., Shimizu, T., Wang, G., 2008. The effect of the particle size of alumina sand on the combustion and emission behavior of cedar pellets in a fluidized bed combustor. Bioresource Technology 99, 3782–3786.

Hanping, C., Bin, L., Haiping, Y., Guolai, Y., Shihong, Z., 2008. Experimental investigation of biomass gasification in a fluidized bed reactor. Energy & Fuels 22, 3493–3498.

Haykiri-Acma, H., Yaman, S., Kucukbayrak, S., 2010. Comparison of the thermal reactivities of isolated lignin and holocellulose during pyrolysis. Fuel Processing Technology 91, 759–764.

Kaewklum, R., Kuprianov, V.I., 2008. Theoretical and experimental study on hydrodynamic characteristics of fluidization in air–sand conical beds. Chemical Engineering Science 63, 1471–1479.

Kaynak, B., Topal, H., Atimtay, A.T., 2005. Peach and apricot stone combustion in a bubbling fluidized bed. Fuel Processing Technology 86, 1175–1193.

Khan, Z., Yusup, S., Ahmad, M.M., Uemura, Y., Chok, V.S., Rashid, U., Inayat, A., 2011. Kinetic Study on Palm Oil Wastes Decomposition. In: Bernardes, M.A.D.S. (Ed.), Biofuel's Engineering Process Technology. InTech, Croatia, pp. 523–536.

Lin, W., Dam-Johansen, K., Frandsen, F., 2003. Agglomeration in bio-fuel fired fluidized bed combustors. Chemical Engineering Journal 96, 171–185.

Park, S.W., Jang, C.H., Baek, K.R., Yang, J.K., 2012. Torrefaction and low-temperature carbonization of woody biomass: evaluation of fuel characteristics of the products. Energy 45, 676–685.

PCD. Pollution Control Department, Ministry of Natural Resources and Environment, Thailand. Air pollution standards for industrial sources. Available from: http://www.pcd.go.th/info_serv/reg_std_airsnd03.html (accessed April 8, 2013).

Permchart, W., Kouprianov, V.I., 2004. Emission performance and combustion efficiency of a conical fluidized-bed combustor firing various biomass fuels. Bioresource Technology 92, 83–91.

Qian, F.P., Chyang, C.S., Huang, K.S., Tso, J., 2011. Combustion and NO emission of high nitrogen content biomass in a pilot-scale vortexing fluidized bed combustor. Bioresource Technology 102, 1892–1898.

Sun, Z., Jin, B., Zhang, M., Liu, R., Zhang, Y., 2008. Experimental studies on cotton stalk combustion in a fluidized bed. Energy 33, 1224–1232.

Sun, Z., Shen, J., Jin, B., Wei, L., 2010. Combustion characteristics of cotton stalk in FBC. Biomass and Bioenergy 34, 761–770.

Turns, S., 2006. An Introduction to Combustion. McGraw-Hill, Boston.

USDA. United States Department of Agriculture. Foreign Agricultural Service. Available from: http://www.fas.usda.gov/psdonline/psdreport.aspx?hidReportRetrievalName=BVS&hidReportRetrievalID=918&hidReportRetrievalTemplateID=1#ancor (accessed April 8, 2013).

Van Caneghem, J., Brems, A., Lievens, P., Block, C., Billen, P., Vermeulen, I., Dewil, R., Baeyens, J., Vandecasteele, C., 2012. Fluidized bed incinerators: design, operational and environmental issues. Progress in Energy and Combustion Science 38, 551–582.

Varol, M., Atimtay, A.T., 2007. Combustion of olive cake and coal in a bubbling fluidized bed with secondary air injection. Fuel 86, 1430–1438.

Varol, M., Atimtay, A.T., Bay, B., Olgun, H., 2010. Investigation of co-combustion characteristics of low quality lignite coals and biomass with thermogravimetric analysis. Thermochimica Acta 510, 195–201.

Wang, C., Wang, F., Yang, Q., Liang, R., 2009. Thermogravimetric studies of the behavior of wheat straw with added coal during combustion. Biomass and Bioenergy 33, 50–56.

Werther, J., Saenger, M., Hartge, E.U., Ogada, T., Siagi, Z., 2000. Combustion of agricultural residues. Progress in Energy and Combustion Science 26, 1–27.

Winter, F., Wartha, C., Hofbauer, H., 1999. NO and N_2O formation during the combustion of wood, straw mault waste and peat. Bioresource Technology 70, 39–49.

Yang, Z., Zhang, S., Liu, L., Li, X., Chen, H., Yang, H., Wang, X., 2012. Combustion behaviours of tobacco stem in a thermogravimetric analyser and a pilot-scale fluidized bed reactor. Bioresource Technology 110, 595–602.